DOI 10.1515/htmp-2012-0087 — High Temp. Mater. Proc. 2012; 31(4-5): 501–511

Diletta Sciti, Laura Silvestroni, Laura Esposito, Kunihiko Nakashima, Noritaka Saito, Yoshinori Yamaoka and Andreas M. Glaeser*

Advances in Transient-Liquid-Phase Bonding of Ultra-high Temperature ZrC Ceramics

Abstract: Full exploitation of the many attractive engineering properties of ultra-high temperature ceramics (UHTCs) requires that they can be joined. This paper explores progress in identifying joining strategies based on the use of transient liquid phases (TLPs). Wetting studies are used to explore the suitability of specific liquids for joining, while bonding studies provide the ultimate test. Sintering aids in the UHTC provide a major potential obstacle to successful joining, and dissolved impurities in the TLP can also complicate the joining process. Nonetheless, we show that well-bonding interfaces can be achieved when ZrC ceramics are bonded at 1673 K using a Ni/Nb/Ni multilayer interlayer.

Keywords: Transient-Liquid-Phase Bonding, wetting, ZrC

PACS® (2010). 81.05.Je, 81.20.VJ, 83.80.Ab

Diletta Sciti: CNR – ISTEC, Institute of Science and Technology for Ceramics, Via Granarolo, 64 I-48018 Faenza Italy
Laura Silvestroni: CNR – ISTEC, Institute of Science and Technology for Ceramics, Via Granarolo, 64 I-48018 Faenza Italy
Laura Esposito: CNR – ISTEC, Institute of Science and Technology for Ceramics, Via Granarolo, 64 I-48018 Faenza Italy
Kunihiko Nakashima: Department of Materials Science & Engineering, Kyushu University, Fukuoka, Japan
Noritaka Saito: Department of Materials Science & Engineering, Kyushu University, Fukuoka, Japan
Yoshinori Yamaoka: Department of Materials Science & Engineering, Kyushu University, Fukuoka, Japan
***Corresponding author: Andreas M. Glaeser:** Department of Materials Science & Engineering, University of California, Berkeley, CA USA, E-mail: aglaeser@sapphire.berkeley.edu

1 Introduction

The ultra-refractory carbides, of which ZrC is an example, are crystalline compounds based on a host metal that is generally arranged in a close-packed structure and carbon that occupies specific interstitial sites within that structure [1–3]. These compounds are also referred to as interstitial carbides and are members of the larger family of ultra-high temperature ceramics (UHTCs). The interstitial nature of the structure leads to a combination of metallic, covalent and ionic bonds. As a result, these carbides exhibit the physical properties of ceramics and the electronic properties of metals, *i.e.*, high hardness and strength with high electrical conductivity. Furthermore, they have the highest melting points (well above 3273 K) of any group of materials, and display high thermal and chemical stability [4] that are useful in aggressive environments.

Although the interesting properties of this class of materials have been known for several decades, the development of practical methods of preparing dense UHTCs in bulk form with desirable microstructures and properties has been a more recent breakthrough. The discovery and use of a wide range of sintering aids has substantially reduced the processing temperatures and pressures required to achieve useful densities, and thus has made these materials much more accessible [5–6]. Understandably, this has sparked a surge of interest in the more widespread use of such materials in a wide range of applications. One current area of intense interest for use of UHTCs is as rocket nozzles and leading edges in aerospace applications. However, additional areas of interest include their use (especially ZrC) in Generation IV very high temperature nuclear reactors (VHTRs) and in solar absorbers in novel high-temperature concentrating solar power systems.

Although one can contemplate making large simply shaped monolithic pieces of these materials, their more widespread use, their use in large components of complex shape, and their more selective and targeted introduction into multimaterial structures will require that they be joined to themselves or to dissimilar materials. The very factors that make the materials attractive for applications can complicate their joining. Many joining methods are available, but relatively few are applicable and lead to high-performance joints with potential for high-temperature service. The relative advantages and disadvantages of the competing joining approaches have been the subject of many papers [e.g., 7–9]. Solid-state diffusion bonding, with or without interlayers, allows the fabrication of refractory joints. Thermal expansion mismatch can be eliminated (self-joining) or can be minimized by

suitable choice of interlayer. Thus in principle, it is possible to produce joints free of substantial residual stress with high-temperature capability. However, both with and without an interlayer, the bonding temperatures are frequently high, the bonding pressures can be substantial, and surfaces must be meticulously prepared to limit the volume of material that needs to be transported to eliminate gaps/voids along the interface and assure a high area fraction of contact in the joint region. By contrast, liquid-based approaches such as brazing exploit the ability of a wetting liquid to flow into and rapidly fill interfacial gaps, and thus offer the potential to allow rapid formation of joints with less-demanding surface preparation requirements [e.g., 9–11]. Although selected reactive-metal brazes, notably Cusil ABA™ (an alloy based on the Cu-Ag eutectic), have seen widespread use, the development of alloys suitable for high-temperature use is more difficult, and in general, the brazing temperature must then exceed the desired use temperature if the brazed joint is to remain solid and be at a suitably low fraction of its remelt temperature during service. These difficulties, and a desire to mitigate residual stresses due to thermal-expansion mismatch have encouraged exploration of methods that utilize a *transient* liquid phase (TLP) as the joining media [11].

In principle, TLP bonding of ceramics has the potential to join high-temperature, high-performance materials at significantly reduced temperatures relative to brazing and solid-state diffusion bonding, in processing cycles that are short in duration (comparable to those in brazing) [12–15]. The extension of TLP bonding to ceramics employs a multilayer (A/B/A) interlayer. A minor portion of the interlayer (A) generates the TLP, and the major portion (B) remains solid during joining, and provides the sink for the liquid former. By choosing a major component, the core layer, with a high melting point and a good thermal expansion match with the ceramic, a refractory alloy that minimizes residual stresses is expected to evolve during processing and use. In order for the approach to be successful, there needs to be a synergistic interaction between several features or characteristics of the interlayer system. The outer cladding layer material must promote the formation of a liquid at reduced temperature. Phase diagrams can provide guidance on this issue. The liquid that forms will generally include some of the core layer due to dissolution, and can similarly interact with the ceramic being joined. The resulting liquid is thus at least a binary and can include additional components. Ideally the wetting characteristics and volume of the liquid are such that all of the interfacial gaps are completely filled, producing a well-bonded interface. Extensive reaction with the ceramic or sintering aids therein is not necessarily desirable, particularly if it leads to the formation of brittle intermetallics or substantially increases the amount of liquid. Ideally, once the liquid has formed and filled interfacial gaps, the liquid former (A) diffuses rapidly into the core layer (and/or adjoining ceramic) causing a progressive decrease in liquid volume at the joining temperature, and ultimately complete isothermal solidification of the joint. As a result, and particularly if extensive redistribution and dilution of the melting point depressant occurs, the remelt temperature of the joint can be several hundred degrees above the original joining temperature, which is obviously advantageous for high-temperature applications. Creating an interlayer that meets all of these criteria simultaneously is challenging, and experiments that are intended to examine individual aspects of the process can often be difficult.

In this study, a Ni/Nb/Ni interlayer, which exhibits many desirable features for TLP bonding, was used to join ZrC ceramics [16]. Liquid formation can initiate in the Ni-Nb system at as low as 1448 K [17]. At higher temperatures, *e.g.*, the joining temperature used here (1673 K), the liquid in equilibrium with Ni-saturated Nb would contain ≈ 58 at% Nb. In practice, this liquid also interacts with the ceramic. In the case of Al_2O_3, the dissolution of the ceramic is minimal [18], however, in the case of carbides (and borides) dissolution can have important influence on the liquid volume and composition, the path of phase evolution, the final microstructure and the joint properties. In this study, we compare joints prepared under otherwise identical conditions using ZrC densified with and without sintering aids that can interact with the liquid.

2 Experimental procedure

2.1 Ceramics preparation

The ZrC powder used to prepare material without sintering aids was Grade B, from H. C Stark (Karlsruhe, Germany) with a mean particle size of 3.5 μm, and a particle size range from 0.8 to 6.0 μm. Information on the purity and other characteristics is provided in Table I. Hf is the prevalent metallic impurity (<2 wt%), but is expected to be in solid solution, *i.e.*, one forms a Zr-rich (Zr,Hf)C. The material also contains up to 1.5 wt% free carbon, which is expected to keep the ZrC at the C-rich phase boundary and/or react with other constituents in the material during sintering, wetting, or joining experiments. For the material prepared with a sintering aid, 15 vol% of tetragonal

Powder	Crystal structure	Supplier	Mean particle size (μm)	Particle size range (μm)	BET (m^2/g)	Purity (%)	Impurities: (wt%)
ZrC	Cubic	Grade B, H.C. Starck, Karlsruhe, Germany	3.8	0.8–6.0	–	–	C_{free}: <1.5 O: <0.6 N: <0.8 Fe: <0.05 Hf: <2
$MoSi_2$	Tetragonal	Aldrich, Milwaukee, WI, USA	2.8	0.3–0.5	1.6	>99	O: <1

Table I: Characteristics of the starting powders used to produce the ceramics.

Sample	HP (K/min)	Density (%)	Mean grain size (μm)	Secondary phases	σ (MPa)
ZrC	2203/60	98	6	C	407 ± 38
ZrC + $MoSi_2$	2173/12	99.2	4	SiC, $MoSi_2$	

Table II: Sintering parameters, microstructural features and 3-point bend strength of bulk ceramics.

$MoSi_2$ (Aldrich, Germany) with a mean particle size of 1 μm, a particle size range of 0.1–2 μm and a specific surface area of 1.6 m^2/g containing <1 wt% O was added to the aforementioned ZrC powder. The powder mixture for the composite was ball milled for 24 h in absolute ethanol using SiC milling media. Subsequently the slurry was dried in a rotating evaporator and the powder sieved through a 60-mesh screen.

Hot-pressing of both materials was conducted in low vacuum (~100 Pa) using an induction-heated graphite die with a constant uniaxial pressure of 30 MPa, with a heating rate of 30 K/min. The pure ZrC was heated to and held at 2203 K for 1 h. The ZrC-$MoSi_2$ composite sample was heated to 2173 K and held for 12 min. Due to the excess (free) C in the ZrC, a portion of the $MoSi_2$ was converted to SiC during densification [19]. For both materials, power to the furnace elements was then turned off and samples underwent free cooling to room temperature.

The sintering parameters, microstructural characteristics and three-point bend strengths of the resulting polycrystalline materials used for the joining experiments are summarized in Table II. Bulk densities were measured by the Archimedes' method on a hydrostatic balance and the microstructural and microchemical characteristics were evaluated on polished surfaces using a combination of X-ray diffraction (Siemens D500, Germany) using the CuK_α radiation, with 0.04° 2θ-step size and 1 s scan step time, scanning electron microscopy (SEM, Cambridge S360, Cambridge, UK) and energy-dispersive x-ray spectroscopy (EDS, INCA Energy 300, Oxford Instruments, UK). Microstructural parameters, like the mean grain size, the volume fractions of residual porosity or secondary phases, were determined through image analysis on micrographs of polished surfaces using commercial software (Image Pro-plus 4.0, Media Cybernetics, Silver Springs, USA). Mean linear intercepts are reported as a measure of the average grain size.

2.2 Interlayer and joint fabrication

The multilayer interlayer consisted of a 125-μm thick Nb core layer sandwiched between 2-μm thick Ni cladding layers. To prepare the interlayer, a 20 mm by 20 mm piece of 125-μm thick 99.7 at% pure Nb foil (Goodfellow Corp., Oakdale, PA) was sectioned, cleaned in solvents and dried and then placed into a physical-vapor-deposition chamber. The Ni source was provided by small pieces of 99.95 at% pure Ni wire (Goodfellow Corp., Oakdale, PA) that were cleaned prior to being inserted into Al_2O_3-coated W-wire baskets in the deposition system. The chamber was evacuated to $<1.3 \times 10^{-4}$ Pa. The Ni sources were then heated and melted under vacuum to induce evaporation. The resulting vapor deposited onto the exposed face of the Nb foil. The foil was then turned over, the wire baskets reloaded, and the process was repeated to coat the second side of the foil.

Sets of rectangular pieces with a roughly 1 cm^2 footprint were cut from larger sintered pellets of the ZrC and ZrC-$MoSi_2$ composite and bonding surfaces were polished to an optical finish using progressively finer grit size diamond pastes, finishing with 0.25 μm paste. The substrates were cleaned using successive baths of acetone and ethanol, and then dried. Pieces of the multilayer foil were then placed between the polished carbide surfaces, the assemblies loaded into an Al_2O_3 crucible and covered with Al_2O_3 milling media to provide a light contact pressure (<1.3 kPa) and limit shifting and misalignment of the joint assembly.

The crucible was then placed into a "clean" cold-wall furnace with Mo and W shields and heating elements operating under high vacuum (10^{-4} Pa) conditions. The samples were heated at 4 K/min to 1673 K, held at the bonding temperature for 30 min and then cooled at 4 K/min to room temperature.

2.3 Wetting studies

High purity powders of Ni (99.99 at%, Sigma-Aldrich Japan, Tokyo, Japan) and Nb (99.9 at%, Nilaco, Tokyo, Japan) were mixed to form an alloy of the lowest melting point (eutectic composition in the Ni-Nb binary, specifically the 59.1Ni-40.9Nb(at%) composition. The powder batch was placed in a crucible of 99.6 at% purity alumina (SSA-S, Nikkato, Osaka, Japan), heated to 1973 K under 10^{-5} Pa vacuum, and held for 30 min to allow complete melting and mixing. A piece weighing ≈0.1 g was machined from the quenched Ni-Nb alloy and rinsed with 1:1 H_2O:HNO_3 for 10 sec to remove surface oxide just before the wetting experiment.

The ZrC substrates for sessile-drop experiments were approximately 10 mm × 10 mm × 3 mm. These plates were polished and cleaned in the same manner as the ZrC blocks that were joined. A small piece of the alloy was placed on top of each type of ZrC substrate and loaded in a high-vacuum, graphite-element furnace. The furnace consists of a graphite stage for the sample and a sapphire window to allow in-situ measurements of the wetting angle. The furnace was heated at 4 K/min to 1673 K and kept for 30 min while a digital camera was used to capture images of the droplet on the substrate in 5–10 K intervals on heating and in 30-sec intervals at 1673 K.

2.4 Characterization

To assess the microstructural characteristics and the spatial variations in composition that evolved during the bonding cycle, the joined pieces were sectioned, polished and analyzed using SEM and EDS analyses, respectively. For the wetting studies, cross-sections of the sessile-drop/substrate interface were also examined using SEM and EDS analysis.

3 Results & discussion

3.1 As-sintered microstructures

Typical microstructures of the monolithic pure ZrC sample and the ZrC-$MoSi_2$ composite after the hot pressing cycles are provided in Figure 1.

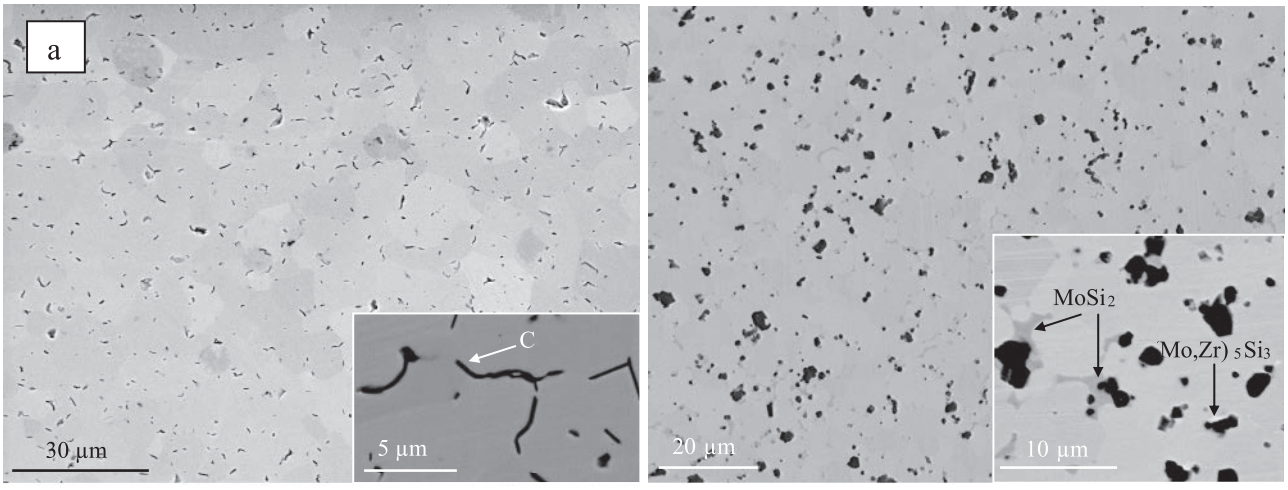

Fig. 1: Polished SEM images of a) monolithic ZrC and b) ZrC-$MoSi_2$ composite. The insets in a) and b) show graphite inclusions in ZrC and $(Mo,Zr)_xSi_y$ phases around SiC in the ZCM composite.

The final density of the monolithic pure ZrC was 98% and x-ray diffraction identified only pure stoichiometric carbide phase. This contrasts with a density of 73% when the material was fired for 1 h at 2223 K without any applied pressure [19]; the application of a pressure was thus necessary to achieve a closed-pore final-stage microstructure. The microstructure was spatially uniform and consisted of generally rounded equiaxed grains with mean grain dimensions in the range of 5–7 μm (Figure 1a). About 2 vol% of very fine closed porosity with pore dimensions in the range 0.3–1 μm was observed; the black phase observed in the polished surface and evident in the Figure 1a inset was graphite present at around 8 vol%, due to the free C in the starting powder.

The ZrC-$MoSi_2$ composite achieved a final density of 6.22 g/cm^3. The crystalline phases detected after sintering were cubic ZrC, β-SiC and a small amount of tetragonal $MoSi_2$. An example of the polished surface is shown in the scanning electron microscope image of Figure 1b. SEM analyses revealed almost no residual porosity. The bright phase corresponds to ZrC grains, which have a mean grain size of 4 μm and a rounded equiaxed shape. The dark agglomerates, present at roughly 10 vol%, are SiC particles, often embedded within $MoSi_2$, which appears as a grey phase with irregular shape (see inset of Figure 1b). The amount of $MoSi_2$ detected by image analysis after sintering was around 5 vol%. Estimating the final composition as 85 vol% ZrC + 10 vol% SiC + 5 vol% $MoSi_2$, the theoretical density calculated using the rule of mixtures is 6.27 g/cm^3, which then yields a relative density of 99.2%.

In prior SEM and TEM studies [6, 19] the formation of SiC was attributed to the reaction between $MoSi_2$ and residual carbon present in the starting ZrC powder. A simple reaction that could describe this transformation is:

$$5MoSi_2 + 7C = Mo_5Si_3 + 7SiC \quad (1)$$

Reaction 1 foresees the formation of Mo_5Si_3. As a matter of fact, at the ZrC-$MoSi_2$–SiC interface, mixed $(Zr,Mo)_xSi_y$ phases with bright contrast and a metal-to-silicon stoichiometry close to 5:3 were detected by EDS.

Alternatively, Mo released during formation of SiC could also enter the ZrC lattice as previously observed for other UHTCs sintered with $MoSi_2$ [19, 20]. EDS spectra recorded from ZrC grains revealed a Mo:Zr ratio of ≈ 4:96, or 4 at% on the cation sublattice. Prior studies confirmed that Mo has solubility in ZrC from 1.1 to 9.4 at% [20]. On the other hand, the presence of Zr peaks was detected in the $MoSi_2$ EDS spectra, indicating a mutual interdiffusion of Zr and Mo into the adjacent phases.

3.2 Wetting studies

Images of the sessile drop taken on the ZrC ceramic are shown in Figure 2. It is evident from the transition in shape between 1373 K and 1473 K that melting occurs in this temperature range, consistent with an anticipated melting temperature of the binary alloy of 1448 K. When the experiment is repeated using ZrC-$MoSi_2$, as shown in Figure 3, melting again initiates between 1373–1473 K, and appears to be nearly complete by the time 1473 K is reached. There is no obvious time/temperature-dependent shift in the contact angle, suggesting that any dissolution of the substrate and resulting change of composition and contact angle occur very early in the process. The two contact angles differ significantly. For the case of pure ZrC, the contact angle remains obtuse, with a final value of 124°.

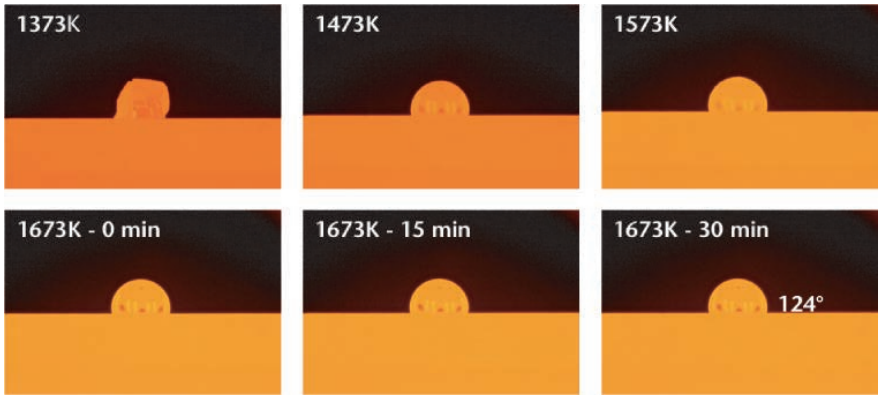

Fig. 2: Images of the Ni-Nb sessile drop on ZrC. Temperatures and holding times at 1673 K are shown, and the contact angle was 124° at the end of the wetting experiment.

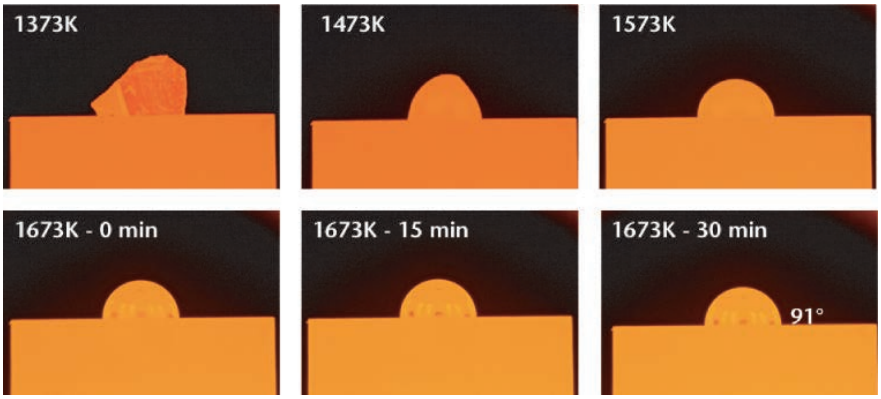

Fig. 3: Images of the Ni-Nb sessile drop on ZrC-$MoSi_2$ material. Temperatures and holding times at 1673 K are again shown. A final contact angle of 91° was reached.

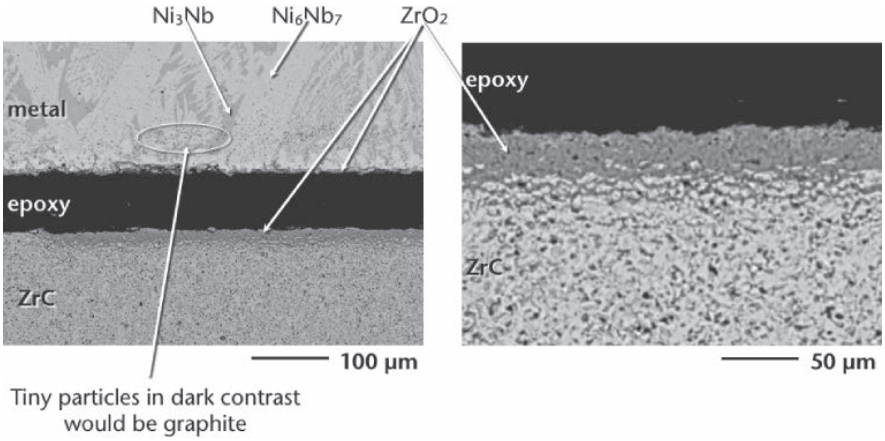

Fig. 4: SEM images of the interface between the solidified Ni-Nb sessile drop and ZrC, showing both the expected intermetallic phases in the metal, but also the development of a ZrO_2 layer between the metal and ZrC. Note the carbon on the metal side of the reaction layer.

By contrast, for the ZrC-$MoSi_2$ material, a final contact angle of 91° is reached.

In conventional ceramic-ceramic brazing, where the liquid would be in contact with ceramic on *both* sides of the joint, a contact angle <90° would be necessary [22]. Thus, neither of these contact angles would be sufficiently low to produce an adequate joint via conventional brazing. One of the advantageous features of the multilayer interlayer is that during joining, the liquid is sandwiched between a solid metal on one side, the core layer, and the ceramic on the other. The tendency of the liquid to flow and fill gaps hinges on the *sum* of the two distinct contact angles. Since in liquid metal–solid metal systems contact angles are generally <60°, a contact angle sum of <180° would be expected, and thus the wetting results do not preclude successful joining using a TLP approach. Nonetheless, to assure the filling of flaws on the ceramic side, it is generally desirable to further reduce the contact angle on the ceramic. Samsanov *et al*. studied the wetting of *pure* Ni on a range of carbide materials [23]. For ZrC, the contact angle was reported as 32° at 1723 K, with the contact angle only weakly dependent on the porosity in the range of porosity relevant in the current study. Thus, to some extent the measured contact angles of 124° and 91° were higher than expected.

EDS analysis of the cross section provided some useful insight on the potential cause of the observed contact angle. As shown in Figure 4a, SEM and EDS analysis shows that the solidified droplet in contact with ZrC contains the expected Ni_3Nb and Ni_6Nb_7 phases suggested by the binary phase diagram [17]. (In TLP bonding, the Nb core layer allows the composition of the liquid to be further enriched in Nb, and thus the composition of the liquid present during TLP bonding will differ somewhat from that examined here.) However, the key observation is the formation of a layer identified as ZrO_2 along the

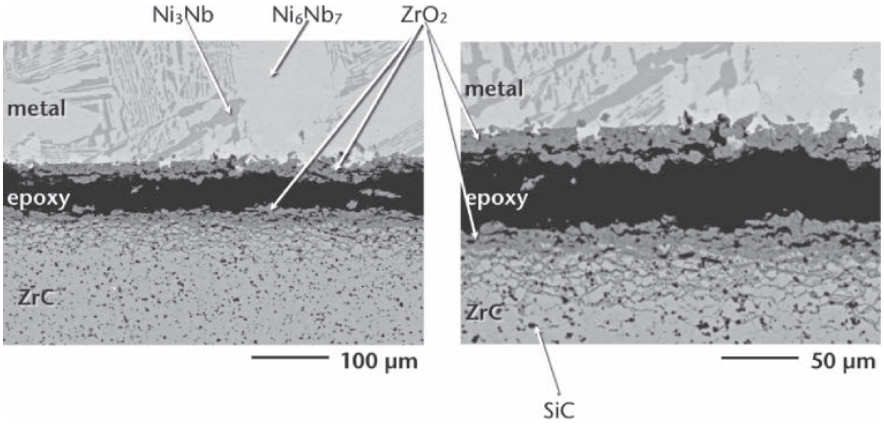

Fig. 5: SEM images of the interface between the solidified Ni-Nb sessile drop and ZrC-$MoSi_2$, again showing the expected intermetallic phases in the metal, and the development of a ZrO_2 layer between the metal and ZrC.

droplet/substrate interface. Since no oxide phases were found in the bulk ceramics, and the oxide layer does not appear to extend beyond the perimeter of the drop, the findings suggest that the liquid metal provided the oxygen source. Qualitatively similar observations are made for the sessile drop on the ZrC-$MoSi_2$ material in Figure 5; the expected Ni-Nb phases are found and a ZrO_2 layer is present.

It is well known that solid Nb in contact with Al_2O_3 at elevated temperatures dissolves Al_2O_3 and that if stoichiometric dissolution occurs that Nb dissolves a substantial amount of oxygen. It is possible that during preparation of the Ni-Nb alloy, similar dissolution occurred, and that the alloy itself then served as an inadvertent source of oxygen. When wetting initiates, the oxygen would be mobile and could be both drawn from the droplet at the liquid surface, but also participate in a reaction at the solid-liquid interface. This points out a challenge in using sessile drop experiments when assessing the behavior of alloys that will participate in a TLP bonding process of the type described. In general, the droplet volume to interfacial contact area ratio will be much larger in the sessile drop experiment than in the actual joining experiment. This increases the volume of the impurity reservoir, conceivably dissolved oxygen in the present case, and the absence of the metal core layer, Nb in the present case, further limits the competition for the impurity. The findings suggest that it may prove beneficial to perform sessile drop experiments in which the volume to interfacial area ratio is varied, and to indeed consider experiments where the sessile drop is of a height more nearly comparable to that of the liquid films used in such TLP joining configurations.

3.3 Joining studies and joint microstructures

In TLP bonding, the interaction between the interlayer and the ceramic can be and often is complex. In a simplified view of the process, the first critical interaction occurs when the first liquid is formed, and in the present case, this is assumed to be when liquid formation initiates at the Ni/Nb interface. When the liquid forms, it is expected that some dissolution of both the core layer and the ceramic, ZrC in this case, occur. Ideally, the liquid has a sufficiently low contact angle on the solid Nb-rich core layer and the ZrC ceramic to flow and fill interfacial gaps. In part, this is what conventional wetting experiments are designed to assess. If the contact angle on the ceramic is sufficiently low, it is possible for the liquid to penetrate three-grain junctions and form a more extensive transition/reaction layer between the bulk ceramic and the bulk core layer material. This may be advantageous, in the sense that it causes the development of a graded structure. It may be disadvantageous in the sense that it makes liquid disappearance more difficult [16]. Suitably designed wetting experiments can also provide insight on this aspect of the behavior.

The following sections describe the joint microstructures for the ZrC and the ZrC-$MoSi_2$ composite, with specific emphasis on the transition region between the residual unmelted Nb core layer and the polycrystalline carbide that retains the microstructure of the original hot-pressed material.

ZrC Joints – Figure 6 shows the joint microstructure at progressively higher magnifications. At the lowest magnification, Figure 6a, one sees that the original Ni/Nb/Ni structure has evolved due to liquid formation and the

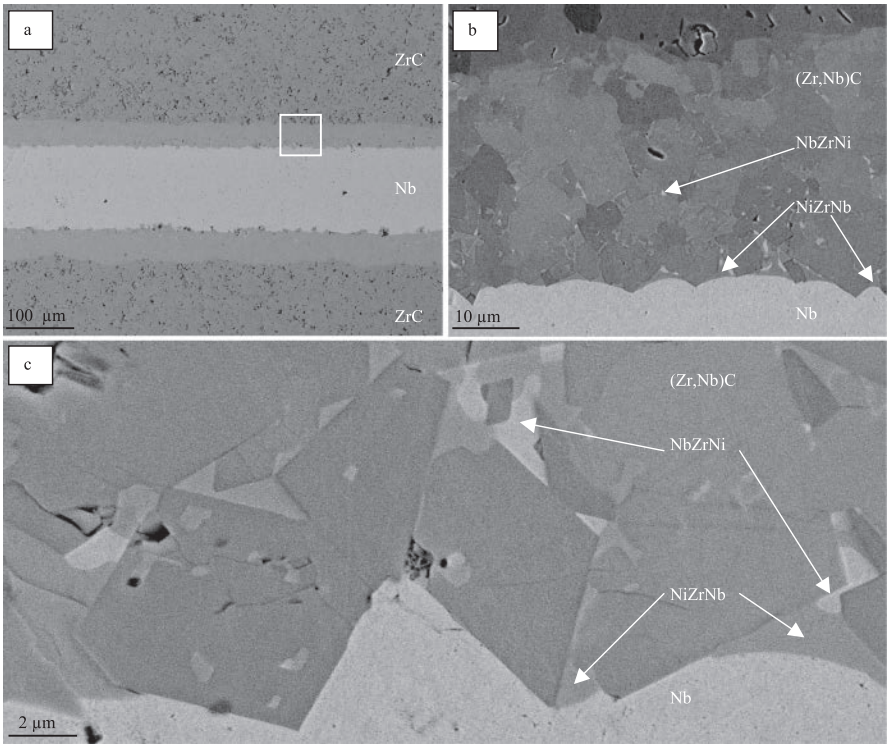

Fig. 6: Polished cross section of the ZrC joint. a) Low magnification, b) and c) magnification of the upper reaction zone as indicated by the squared area in a).

interaction of that liquid with the ZrC. The thickness of the Nb foil has decreased from 125 µm to 115 µm, suggesting dissolution of a 5-µm thick layer from each side of the foil. A roughly 40-µm thick reaction layer has developed, indicating substantial dissolution of and interaction with the carbide occurred. Beyond the reaction zone, the ZrC maintained the microstructure of the as-sintered specimen, suggesting that no degradation of the bulk properties occurred during joining.

Figure 6b provides a higher magnification view of the reaction zone that has developed. EDS analysis indicates that several different phases are present. No evidence of a ZrO_2 layer is found within the reaction layer. Moving from the bulk ceramic towards the interlayer, the first appears to be a solid-solution carbide with an average composition that is roughly $(Zr_{0.65}Nb_{0.35})C$, with Zr:Nb atomic ratio varying from 70:30 to 60:40 as one approaches the Nb foil. It is known that ZrC and NbC can form a complete series of solid solutions [24]. Irregularly shaped pockets of Ni-Nb-Zr alloys containing traces of C were also detected. The volume fraction of these metal regions increased as one moves from the ZrC side of the reaction zone towards the Nb interlayer. The (Zr,Nb)C grains that bound these metal-filled pockets are often highly faceted. EDS analysis of the metal-filled intergranular regions was performed. The most frequently obtained results suggest a composition in which the Ni, Zr and Nb are present in an atomic ratio of 50:35:15, with traces of C also present. This phase is labeled "NiZrNb" in Figures 6b and 6c. A second metallic phase, characterized by a higher Nb content and appearing as a brighter/lighter region in the micrographs is also identified and appears in contact with NiZrNb. EDS of this Nb-rich phase, labeled NbZrNi, suggests an atomic Nb:Zr:Ni ratio of 70:25:5. These two alloys, one Ni-rich and the other Nb-rich, were always found adjacent to one another in a "striped" morphology frequently observed as a result of solidification of a eutectic liquid. In the present case, Zr is incorporated in the liquid and as a result, the compositions differ from those in the Ni-Nb binary diagram. Occasional pockets of unreacted Nb with a rounded morphology and bright contrast were detected along triple junctions close to the Nb side. No residual (free) carbon was observed in the reaction layer. Essentially all the "porosity" was filled by the metallic phases. The penetration of the liquid into porosity in the as-fired material is not what one expect for a liquid with a contact angle of 124° on the ceramic. It is also not expected that a liquid with this high a contact angle would penetrate along three-grain junctions. It thus appears that oxygen impurities in the sessile drop, and the oxide film that

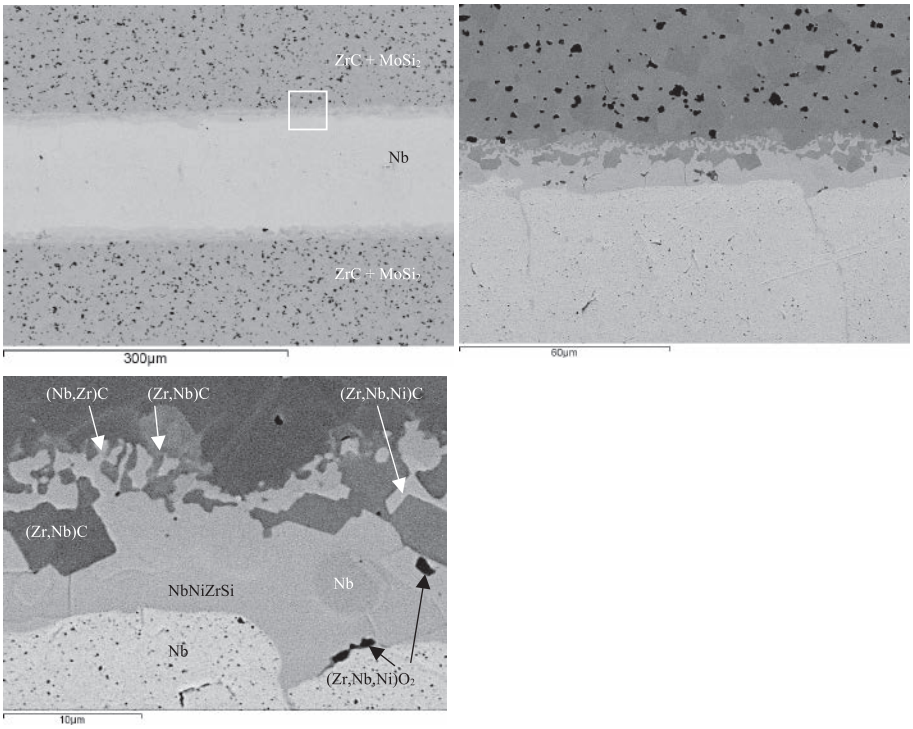

Fig. 7: Polished cross section of the ZrC-$MoSi_2$ joint. a) Low magnification, b) and c) magnification of the upper reaction zone as indicated by the squared area in a). Although a mixed oxide phase was identified, the phase is discrete and present in much more limited amount than in the sessile drop experiments.

developed during the wetting experiments may have had a major effect on the contact angle and the liquid-substrate interaction. Experiments utilizing thinner Ni films will provide insight on whether the reaction zone thickness scales with the Ni film thickness, and whether well-bonded interfaces and thinner transition/reaction layers can be achieved by simply reducing the Ni film thickness. This would be advantageous in that it reduces the amount of Ni in the liquid that ultimately needs to be absorbed by the Nb core layer, and may facilitate isothermal solidification.

ZrC-$MoSi_2$ Joints – The microstructure of the resulting joint between ZrC-$MoSi_2$ ceramics is displayed in Figure 7 and it is evident that despite the increased chemical complexity of the ceramic a well-bonded interface formed. The initial Nb foil was reduced from 125 to 110 µm. A reaction layer roughly 10–18 µm thick provides the transition from the Nb-rich core layer to the bulk ZrC-$MoSi_2$ ceramic, Figure 7a. The bright phase close to Nb was a metallic phase containing Nb, Ni, Zr and Si in relative quantities around 67:12:5:16 at% and this phase showed a tendency to infiltrate the Nb core layer, as shown in Figure 7b. Suggestions of grain boundary penetration of the Nb-Ni liquid along grain boundaries in Nb have been previously observed, and this is currently being investigated in more detail. A 1073 K isothermal section in the ternary Nb-Ni-Si system [25] has three intermetallic phases at 1073 K with a roughly 5:1 metal:silicon ratio. Higher resolution studies, ideally using transmission electron microscopy will be needed to ascertain whether this penetrating alloy is or contains a silicide. Anisotropy in the coefficient of thermal expansion, typical of metal silicides [26], or differences in ductility can be problematic when the joint component is subjected to harsh thermal and mechanical environments. Equivalent channel features were not observed in other pure carbide matrices (ZrC, HfC, TaC) [15], and this may indicate that the introduction of silicon notably alters the equilibrium of these systems. The nature and amount of silicon sources may be an important issue in the design of UHTCs that need to be joined.

The reaction layer contains $(Zr_{0.8}Nb_{0.2})C$ faceted grains with dark contrast and Nb rounded grains with the same contrast as the metal, suggesting that Nb precipitates from the melt during solidification of the residual liquid. Small cracks could be occasionally observed emanating from the larger $(Zr_{0.8}Nb_{0.2})C$ grains, Figures 7b and 7c. As was the case for pure ZrC, these mixed carbide grains have a very pronounced faceted appearance, suggesting they were in contact with liquid. Moving toward the ceramic, irregularly shaped and alternating grains of (Zr,Nb)C were

present (Figure 7c); the Zr:Nb atomic ratio was ≈ 60:40 in the grains with dark contrast, while those with brighter contrast had a 40:60 Zr-Nb ratio. No Ni traces could be deteced by EDS in these two phases of alternating bright and dark contrast. However, Ni was detected in some faceted mixed carbide grains having bright contrast in contact with $(Zr_{0.8}Nb_{0.2})C$ and the two types of jagged (Zr,Nb)C particles. Very dark pockets immersed in the reaction layer visible in Figure 7c were identified as Zr-Nb-Ni oxides. It should be noted that the extent of oxide formation is significantly less than was seen in the sessile drop experiments. Farther away from this reaction zone, ZrC grains of the ceramic did not contain any evident Nb or Ni. Mo was not readily detectable within the joint regions owing to both its presumed low amount and overlaps of its main peaks with those of Zr and Nb.

4 Conclusion

Although there are obvious benefits to the use of sintering aids when processing UHTCs, they also have the potential to affect many aspects of the joining process, and some effects are likely to be detrimental. The results have shown that even when impurities lead to the formation of a ZrO_2 reaction layer that to some extent separates the TLP from the ceramic, there are differences in the wetting behavior. The only obvious variable is the sintering aid. Fortunately, in the case of ZrC ceramics, the limited amount of residual $MoSi_2$ sintering aid does not appear to detrimentally affect the outcome of joining experiments, nor did the SiC that was present. Additional studies exploring the interactions between the TLP and the SiC formed in ZrC prepared with a $MoSi_2$ sintering aid are needed to assess whether the behavior seen in this system, specifically the lack of extensive silicide formation, is more generally true for other UHTC carbides. Longer heat treatments, and subsequent analyses of phase content and microstructure in the joint regions, analyzed in the context of existing thermodynamic information, *e.g.*, [27, 28] would be useful in identifying and distinguishing transient from equilibrium phases, and providing a clearer picture of longer-term joint stability. The outcome is of obvious interest since the inclusion of SiC reinforcement in the form of particles, whiskers or fibers [*e.g.*, 29, 30] in UHTCs is envisioned.

The results indicate that there may be a need to use a broader range of wetting experiments to more closely simulate the volume:interfacial area ratios commonly encountered during TLP bonding. Although there are obvious advantages to using equilibrated prealloyed metals in fundamental studies of spreading kinetics, the potential to inadvertently contaminate the alloy may introduce unwelcome complications. Systematic studies using alloys formed *in situ* may offer advantages, and some insights may be gained from experiments that intentionally vary the sessile drop volume over wide ranges, or where the dewetting of thin films is examined as part of a broader range of experiments.

The results demonstrate the potential of applying a TLP-based approach to joining UHTCs processed with and without a sintering aid, and in the absence of any substantial bonding pressure. In both cases, the interlayer and ceramic are well-bonded, and the interfacial reaction zone is free of the large cracks that have been seen in other efforts to join UHTCs with brazes. Critical tasks that remain are to achieve conditions that allow full disappearance of the liquid, and to assess the strength-temperature behavior of both the present joints and those that achieve full liquid disappearance.

Received: April 30, 2012. Accepted: July 11, 2012.

References

[1] H. O. Pierson in *Handbook of refractory carbides and nitrides*, William Andrew Publishing/Noyes, (2001), p. 55.
[2] L. E. Toth, in *Refractory Materials, A Series of Monographs*, edited by J. L. Margrave, Academic Press Inc., New York, NY, (1971), p. 6.
[3] E. K. Storms, in *Refractory Materials, A Series of Monographs*, edited by J. L. Margrave, Academic Press Inc., New York, (1967), p. 94.
[4] M. M. Opeka, I. G. Talmy and J. A. Zaykoski, *Journal of Materials Science,* **39**, 5887–5904 (2004).
[5] X. Zhang, G. E. Hilmas and W. G. Fahrenholtz, *Journal of the American Ceramic Society*, **90**, (2), 393–401 (2007).
[6] L. Silvestroni and D. Sciti, *Journal of Materials Research*, **26**, [7], 1882–1889 (2008).
[7] K. Suganuma, Y. Miyamoto and M. Koizumi, *Annual Review of Materials Science*, **18**, 33–47 (1988).
[8] G. Elssner and G. Petzow, *ISIJ International*, **30**, (12), 1011–32 (1990).
[9] J. A. Fernie, R. Drew and K. M. Knowles, *International Materials Reviews*, **54**, [5], 283–331 (2009).
[10] L. Esposito and A. Bellosi, *Journal of Materials Science,* **40**, 4445–4453 (2005).
[11] R. E. Loehman and A. P. Tomsia, *Bulletin of the American Ceramic Society,* **67**, (2), 375–380 (1988).
[12] D. S. Duvall, W. A. Owczarski and D. F. Paulonis, *Welding Journal*, **53**, (4), 203–14 (1974).
[13] M. L. Shalz, B. J. Dalgleish, A. P. Tomsia and A. M. Glaeser, *Journal of Materials Science,* **28**, (6), 1673–84 (1993).
[14] J. D. Sugar, J. T. McKeown, S. Hong, T. Akashi, K. Nakashima and A. M. Glaeser, *Journal of the European Ceramic Society*, **26**, (4–5), 363–72 (2006).

[15] L. Silvestroni, D. Sciti, L. Esposito, and A. M. Glaeser, accepted for publication in the *Journal of the European Ceramic Society*.
[16] S. M. Hong, C. C. Bartlow, T. B. Reynolds, J. T. McKeown and A. M. Glaeser, *Advanced Materials*, **20**, [24], 4799–4803 (2008).
[17] T. B. Massalski, H. Okamoto and ASM International, Binary alloy phase diagrams, 2nd Ed. Materials Park, OH: ASM International, 1990.
[18] S. M. Hong, T. B. Reynolds, C. C. Bartlow and A. M. Glaeser, *International Journal of Materials Research*, **101**, (1), 133–142 (2010).
[19] L. Silvestroni, D. Sciti, J. Kling, S. Lauterbach and H-J. Kleebe, *Journal of the American Ceramic Society*, **92**, (7), 1574–1579 (2009).
[20] L. Silvestroni, H-J. Kleebe, S. Lauterbach, M. Müller and D. Sciti, *Journal of Materials Research*, **25**, (5), 828–834 (2010).
[21] S. E. Landwehr, G. E. Hilmas and W. G. Fahrenholtz, *Journal of the American Ceramic Society*, **90**, (7), 1998–2002 (2007).
[22] M. L. Shalz, B. J. Dalgleish, A. P. Tomsia, R. M. Cannon and A. M. Glaeser, *Journal of Materials Science,* **29**, [14], 3678–90 (1994).
[23] G. V. Samsonov, A. D. Panasyuk and G. K. Kozina, *Powder Metallurgy and Metal Ceramics*, **7**, (11), 874–78 (1968).
[24] W. G. Lidman and H. J. Hamjian, *Journal of the American Ceramic Society*, **35**, (9), 236–240, (1952).
[25] E. I. Gladyshevskii, O. S. Koshel', and R. V. Skolozdra, *Inorganic Materials*, **5**, 1882–1884 (1969).
[26] J. J. Petrovic, *Ceramic Engineering and Science Proceedings*, **18**, (3), 3–17 (2008).
[27] M. E. Schlesinger, *Chemical Reviews*, **90**, 607–628 (1990).
[28] T. C. Chou, A. Joshi and J. Wadsworth, *Journal of Materials Research*, **6**, (4), 796–809 (1991).
[29] E. Wuchina, E. Opila, M. Opeka, W. Fahrenholtz and I. Talmy, *The Electrochemical Society Interface*, Winter 2007, 30–36.
[30] L. Silvestroni and D. Sciti, *Journal of the American Ceramic Society*, **94**, (9), 2796–2799 (2011).